Model to predict motion sickness within autonomous vehicles

Salter, S, Diels, C, Herriotts, P, Kanarachos, S & Thake, D

DOI 10.1177/0954407019879785
ISSN 0954-4070
ESSN 2041-2991
Publisher: Sage

Model to predict motion sickness within autonomous vehicles

Spencer Salter[1,2], Cyriel Diels[1], Paul Herriotts1, Stratis Kanarachos[1] and Doug Thake[1]

Abstract

Background: Motion sickness is common within most forms of transport; it affects most of the population who experience varied symptoms at some stage in their lives. Thus far, there has been no specific method to quantify the predicted levels of motion sickness for a given vehicle design, task and route.

Objective: To develop a motion sickness virtual prediction tool that includes the following inputs: human motion, vision, vehicle motion, occupant task and vehicle design.

Method: A time domain analysis using a multi-body systems approach has been developed to provide the raw data for post-processing of vehicle motion, occupant motion and vision, based on a virtual route designed to provoke motion sickness, while the digital occupant undertakes a specific non-driving related task.

Results: Predicted motion sickness levels are shared for a simple positional sweep of a vehicle cabin due to a prescribed motion and task. Two additional examples are shared within this study; first, it was found that the model can predict the difference found between sitting forwards and backwards in an autonomous vehicle. Second, analysis of a respected and independent study into auxiliary display height shows that the model can predict both relative and absolute levels between the two display heights congruent to the original physical experiment.

Conclusion: It has been shown that the tool has been successful in predicting motion sickness in autonomous vehicles and is therefore of great use in guiding new future mobility solutions in the ability to tune vehicle dynamics and control alongside vision and design attributes.

Keywords

Automated vehicle, motion sickness, simulation

Date received: 8 March 2019; accepted: 3 September 2019

Introduction

Most original equipment manufacturers (OEMs) are declaring their intention to be part of a driverless future. Concepts often depict non-conventional seating layouts. One objective of automated vehicles (AVs) is to be able to 'multitask' during a drive and be able to increase the inherent value of that journey. To enable this, many concepts include features that can increase productivity and enjoyment. Indeed, commuter satisfaction is improved regardless of modality if the value of a journey is increased.[1] Furthermore, the 'time–cost' saving for journeys for AVs could be as high as 50% and 80% in some cases.[2] It is, therefore, key to maximise the time available in an AV to be effectively engaged in other tasks. The driving task will in future be automated to manage the motion and flow safely with other road users in a public space, thus, leaving all occupants to be free to multitask. This poses significant challenges, one being able to complete visual tasks while subjected to motion typical of motor vehicles.[3] In addition, reduced performance has been shown when a computer is used within a dynamic environment.[4,5] In another study, it has been shown that lateral motion at 4 Hz was the most difficult for reading and writing tasks and shown to be more difficult using a table rather than lap-based tasks.[6]

It has been argued extensively that the critical challenge to the acceptance of AVs will be motion sickness. Motion sickness is a condition characterised by

[1]Centre for Mobility & Transport, Coventry University, Coventry, UK
[2]Jaguar Land Rover, NAIC, The University of Warwick, Coventry, UK

Corresponding author:
Spencer Salter, Centre for Mobility & Transport, Coventry University, Priory Street, Coventry CV1 5FB, UK.
Email: salters@uni.coventry.ac.uk

symptoms such as (cold) sweating, pallor, flatulence, burping, salivation, apathy and finally by nausea and retching. Motion sickness is known to affect around two-thirds of the population at some point in their lives.[8,9] Motion sickness occurs if the motion as sensed via our sensing systems (i.e. sensed motion) is different from what we expect them to be (i.e. expected motion). For example, when using a mobile device in a car, the stationary visual scene suggests that the body is stationary and is incongruent with the physical motions sensed by the occupant's organs of balance, the vestibular system.

Motion sickness has historically been evaluated using self-report by sufferers using one of the many motion sickness scales available. Fast motion sickness scale (FMS)[10] and MIsery Sickness sCale (MISC)[11] are notable and widely used. All subjective evaluation of motion sickness requires some level of mature physical presentation and therefore outside of rapid digital prototyping.[12]

There is currently active debate on the exact weightings to use within motion sickness research. Most published studies use weightings and methodologies described in standards.[13,14] Recommendations have been made to include lower frequency data for lateral and longitudinal directions.[15]

It has been found that the exterior forward view from within the cabin to be influential in reducing motion sickness.[16] It has also been shown that periph- eral vision is key to the propensity of motion sickness that leads to ergonomic implications for the design and positioning of in-vehicle displays.[17] It has also recently been proven that facing rearwards in urban environments within an AV leads to significantly more motion sickness in occupants than facing forwards.[18]

The task and vehicle design are key to the overall level of anticipatory cues to the future path of the vehicle[19]; this is congruent with earlier studies; in addition, the studies also found that driver expertise played a greater role in the development of motion sickness in passengers than vehicle type.[20] It has also been shown that the smoothness of vehicle control by the driver is a significant factor leading to motion sickness.[21]

There are several internal human models to predict motion sickness in the literature.[22–24] Wada shared a model for comparing passenger and driver head tilt in the context of motion sickness by demonstrating a proposed 6 degrees of freedom model.[25] They concluded that visual signals should also be included. To date, no such models have been demonstrated that are an amalgamation of vision due to occupant and coupled vehicle motion that can be used to assess vehicle designs for motion sickness. This paper is structured to initially define the model including a simple demonstration of a positional sweep of a vehicle interior followed by two real-world examples where validation is proven.

The model represents an original and novel contribution by processing motion, vision and task in the context of human motion sickness. The aim of this study is to demonstrate a novel and useful quantitative motion sickness model that includes provocative stimulus and multi-tasking.

Method

The model is split into three discrete but connected by parts that can be used to generate motion sickness performance metrics. First, the gross motion of the vehicle is considered for a specified route. Second, the biomechanical model of the human completes a defined task within the virtual environment while being driven. The vision that the biomechanical model records from its eyes are processed using unique algorithms leading to a motion sickness score. The later requires a torso, neck and head including eyes and vestibular sensor locations to capture motion altered vision as would be captured by a human. The task chosen for this demonstration is to read a book/tablet, a method often used in motion sickness studies.[17] The model is built and solved using standard modelling elements and within a commercially available code SIMPACK 10.2.1®.

Virtual environment

The target path and vertical disturbances, braking and accelerations are illustrated in Figure 1. This profile has been developed over several iterations that provide enough provocative input within a short amount of time, albeit arbitrary. The inputs demonstrated here could be specified to match any route or physical study using known boundary conditions. The drive contains a rough road section based on physical unpaved road geometry. This excites the vehicle sufficiently for evaluation of non-linearity and/or performance of active systems. Steering and longitudinal control of the vehicle is achieved using the standard driver model using default values within SIMPACK 10.2.1®.[26,27]

The model has an initial speed of 40 km/h and varies according with the braking and throttle applied. The application percentages for brake and throttle refer to power train torque. For example, a powertrain with 500 Nm is varied by the percentage application to simulate an unsteady throttle and engine braking, as shown in Table 1.

The levels used here are used to simulate slight speed deviations in the vehicle speed at sickening frequencies, as shown in Figure 2.

The rough surface yields the following profile (87-mm range, standard deviation (SD) = 7.5 mm, mean = 0.0). The rough section is like off-road tracks that are provocative for motion sickness and useful for task performance studies. The frequency content is illustrated in

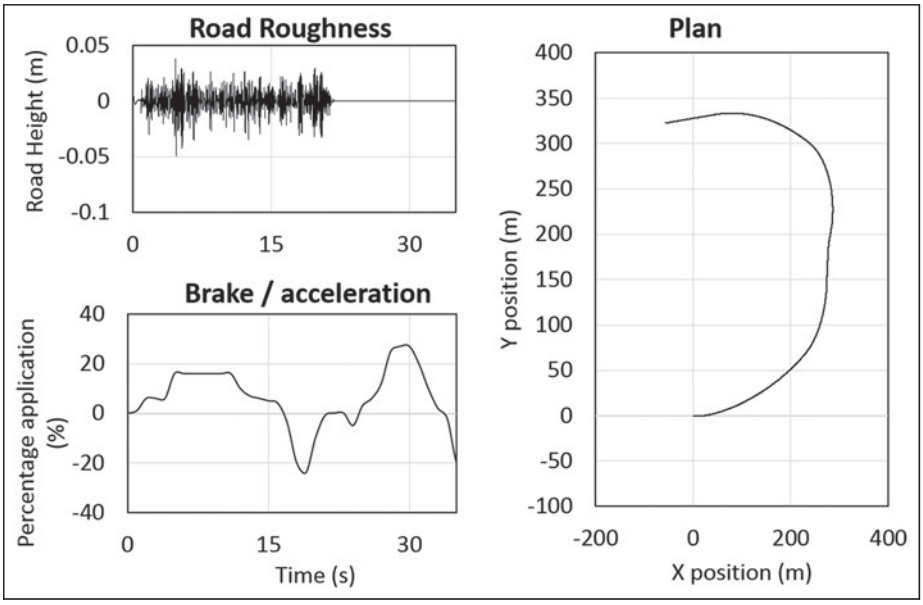

Figure 1. Model inputs, path, longitudinal and vertical excitation.

Table 1. Braking and acceleration description sampled in every 0.078 s.

Acceleration (m/s^2)	Braking	Accelerating
Mean	20.18	0.47
SD	0.40	0.39
n	4914	1459

SD: standard deviation.

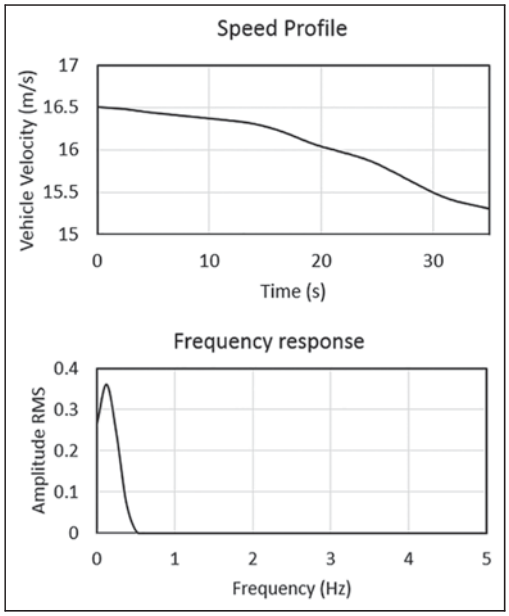

Figure 2. Speed profile (Jaguar XE), deviation in speed from the application of torque (brake/acceleration %) in addition to losses from friction, (top) tyre rolling resistance and aerodynamic forces and (bottom) frequency response of the speed variation (RMS, flat top window, 75% overlap and 0.1-Hz resolution).

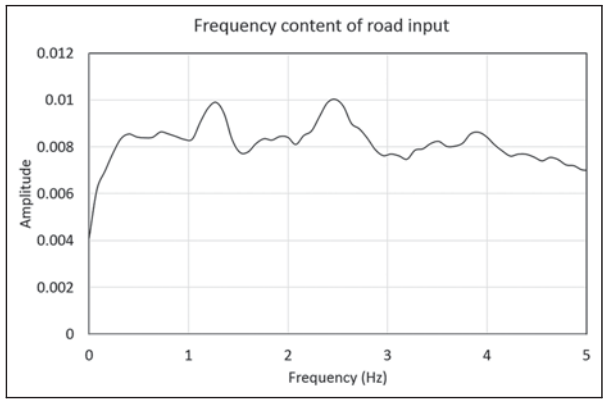

Figure 3. Frequency spectrum of road input (m). (RMS level, flat top window, 75% overlap and 0.1-Hz resolution).

Figure 3 indicating a relatively flat input for primary vehicle response frequencies (\2 Hz).

Vehicle

The model, as shown in Figure 4, builds upon established vehicle dynamics models used in the motor industry.[28,29]

The vehicle model contains more than 500 degrees of freedom that are used to represent the elasto-kinematic suspension, power-unit and transmission. It is known that levels of steering connection and immediacy are an important factor in vehicle handling and low-frequency steering performance of vehicles.[30,31] The steering system is described in enough detail to replicate this. All geometry, bushes and masses are set to nominal design conditions for each specific vehicle line. The body can be either fully flexible to represent flexure for ride comfort or fully rigid for basic handling. The models used

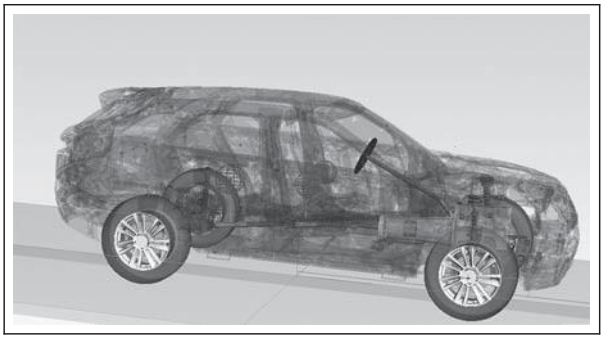

Figure 4. Example model, Range Rover Velar 19 Model Year.

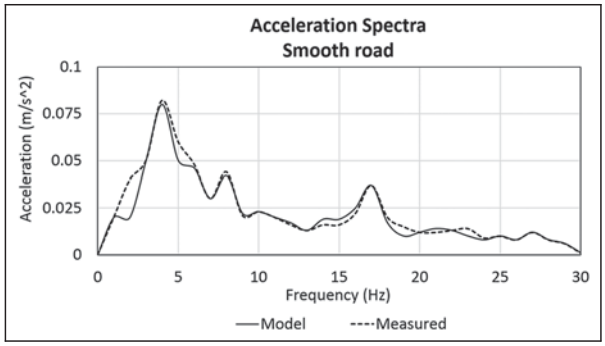

Figure 5. Front seat rail vertical ride spectra, RMS levels (flat top window, 75% overlap and 0.25-Hz resolution) for a smooth UK 'A' road at 60 mile/h.

within this study are all fully rigid for the body and suspension components. The complexity of the model is deliberately low in areas which do not influence the low-frequency motion behaviour of the vehicle. Thus, providing a useful model without carrying the burden of high-fidelity data for unnecessary accuracy.[32] The full fidelity baseline model used within this study correlates well with measured data for vehicle ride comfort (Pearson = 0.97, Mean = 0.021, SD = 0.017, Mean = 0.022, SD = 0.018) for the model and measured vertical ride spectra, respectively, as shown in Figure 5.

Occupant

To facilitate occupant head movement in the cabin, a mechanical head was created using the same multi-body systems (MBSs) formulation as the vehicle model with basic humanoid motion including eye tracking. This allowed easy vision recording within the cabin while undertaking a task during a drive.

Magnetic resonance imaging (MRI) imagery was used to construct the basic geometry of the skull, cervical spine, vestibular system and eye positions. The MRI data were from a 40-year-old 75th percentile UK male (permission granted).

The topology of the assembled digital head is illustrated in Figure 6. The biomechanical model is unique to this analysis. Only head and neck motion are represented (cervical 1–8 vertebrae) to allow head tilt with rotation from the shoulders to facilitate looking around the vehicle cabin. The enforced mechanical motion of the head and neck is intended to point the head towards the eye target. The fine levels of eye tracking vestibular ocular reflex (VOR) are achieved by a closed loop controller on each eye such that the eye points exactly at the target regardless of the head orientation. The connections indicate the joints and forces between each body. The head is connected in series through the cervical vertebrae through to the shoulders. The shoulders are attached to the seat connection point. The corresponding three-dimensional (3D) representation is illustrated in Figure 7.

The stiffness of the neck bushes was optimised to match the transmissibility of a 65th percentile male wearing a steady state accelerometer fixed to spectacles with a ground accelerometer fixed to the adjacent position on the B-post door pillar. The physical measurements were recorded on urban roads that included traffic islands. The model used a constant velocity sine sweep applied to the base of the shoulders and the B-post as the ground disturbance. The head was considered as the free output side, as shown in Figure 8. The cross spectral density was determined for both physical and the model. There was no significant difference between the resulting passive (relaxed) human transmissibility and modelled transmissibility using a t-test ($t = 20.87$, $p < 0.05$, Mean = 0.85, SD = 0.53, Mean = 0.97, SD = 0.366) for the model and human, respectively, as shown in Figure 9.

The relevant equations are equations (1)–(3)

$$m \cdot \underline{v}^b + \underline{v}^b \times m \cdot \underline{v}^b = f^b \qquad (1)$$

where m is mass (kg), v^b is linear velocity (m/s) in body reference frame (Figure 7), v^b is angular velocity (m/s) in body reference frame and f^b is force (N) in body reference frame.

Euler dictates that angular momentum is equal to the applied torque[33]

$$I \cdot \underline{v}^b + \underline{v}^b \times I \cdot \underline{v}^b = t^b \qquad (2)$$

where I^s is inertia tensor (kg/m^2) relative to the inertial frame, v^s is spatial angular velocity (rad/s) and t is externally applied torque (N m).

Combining the above equations leads to the Newton–Euler equation in the body reference frame (equation (4))

$$\begin{bmatrix} m & 0 \\ 0 & I \end{bmatrix} \cdot \begin{bmatrix} \underline{v}^b \\ \underline{v}^b \end{bmatrix} + \begin{bmatrix} v^b \times m \cdot v^b \\ \underline{v}^b \times I \cdot v^b \end{bmatrix} = \begin{bmatrix} f^b \\ t^b \end{bmatrix} \qquad (3)$$

where I is inertia tensor (kg/m^2), f^b is external force (N) applied at the centre of mass and t^b is external torque (Nm) applied at the centre of mass.

The model used here employs relative kinematics and as such the equations of motions in each kinematic chain are described relative to one another. The position and velocity are a result of the generalised joint coordinates of the preceding bodies within the series,

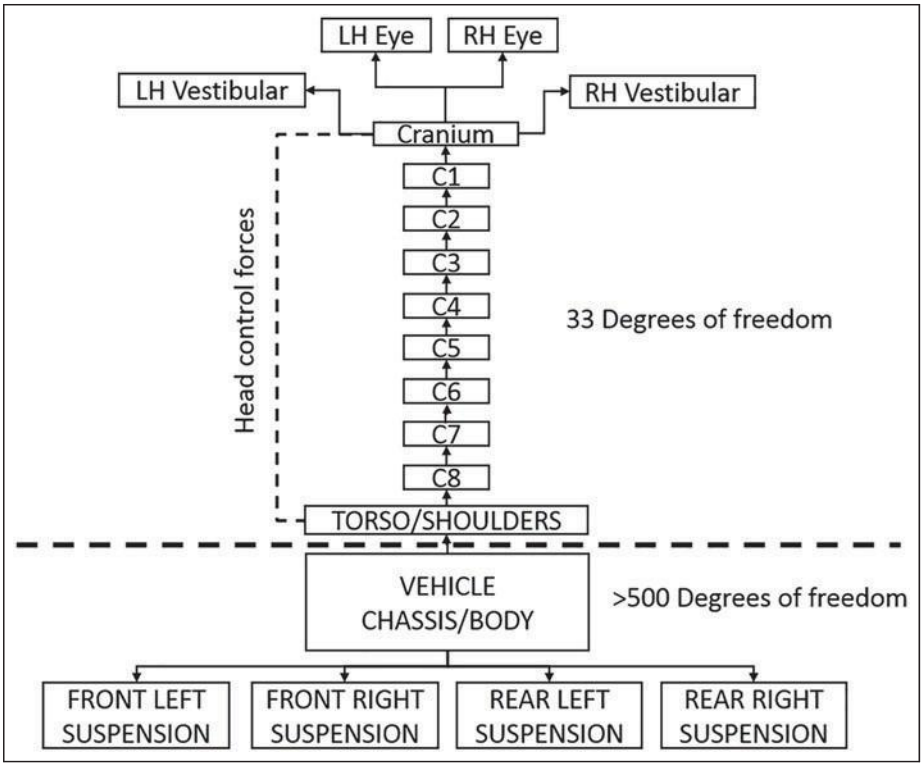

Figure 6. Head and torso 2D topology, each block within the vehicle section represents a substructure containing the detailed content for joints and associated connections.

The shoulders connect to the seat point; the head has flexibility from the bushes that mimic the cervical discs. Head motion is facilitated by rotation of the head to cervical C1 connection and four force actuators from the head to the shoulders. Eye motion is achieved by tracking a target point with the x-axis of the eye joint. The target forms part of the non-driving related task and used to direct the gaze of the virtual occupant.

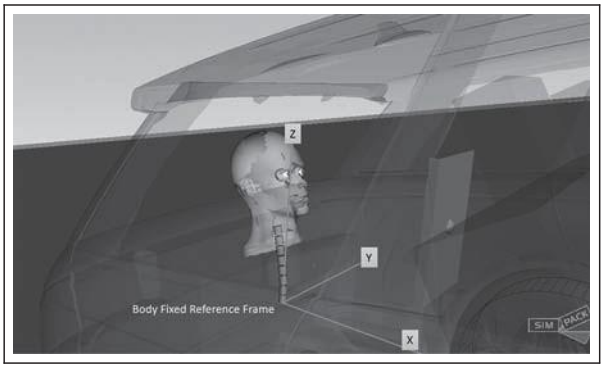

Figure 7. Head and torso 3D representation.

for example, the assembly joint between the 'from' marker M_{i21} of body i2 1 to the 'to' marker M_i is coincident with the body reference frame R_i and leads to the following equations (equations (4)–(9))

$$A_{M_{i-1}R_i} = A_{M_{i-1}R_i}(q_i, t) \quad (4)$$

$$r_{M_{i-1}R_i} = r_{M_{i-1}R_i}(q_i, t) \quad (5)$$

where A is the orientation and r is the position

$$v_{M_{i-1}R_i} = J_{v_i}(q_i, t) \cdot \dot{q} + v_{M_{i-1}R_i}(q_i, t) \quad (6)$$

$$M_{i-1_{r_{M_{i-1}R_i}}} = J_v \dot{q}_i, t) \cdot \dot{q} + M_{i-1}\dot{r}_{M}^{i-1}{}_{R}\dot{q}_i, \dot{q}\, t) \quad (7)$$

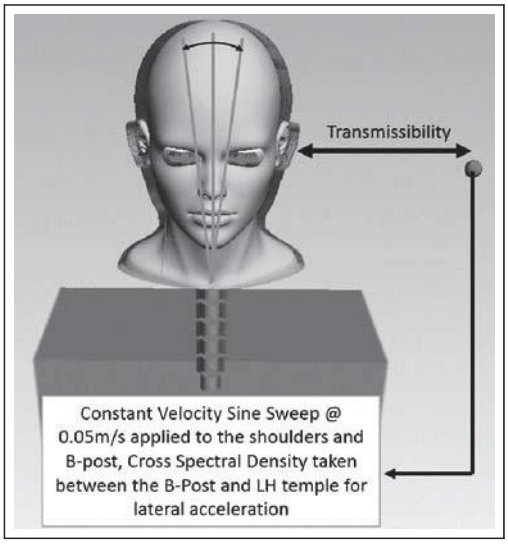

Figure 8. Cross spectral density (CSD) optimisation method, CSD taken between the LH temple position on the model and an adjacent point on the body (small ball).

where v is the angular velocity and M is the linear velocity

$$M_{i-1_{v_{M_{i-1}R_i}}} = J_v(q_i, t) \cdot \dot{q} + M_{i-1}v_{M_{i-1}R_i}(q_i, \dot{q}\, t) \quad (8)$$

$$M_{i-1_{\omega_{M_{i-1}R_i}}} = J_{v_i}(q_i, t) \cdot \dot{q} + M_{i-1}r_{M_{i-1}R_i}(q_i, t) \quad (9)$$

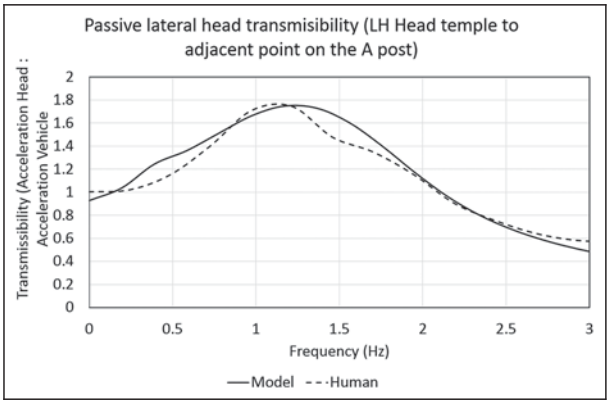

Figure 9. Comparison of head transmissibility for the model and equivalent physical measure.
Cross spectral density between the head position (left temple) to an adjacent point on the left hand B-pillar close to the upper seat belt anchor. Physical stimuli were an urban road containing a road traffic island. Model stimuli used a constant velocity sine sweep with an amplitude of 0.05 m/s.

where $M_{i-1_{\underline{v}\,M_{i-1}R_i}}$ is the angular acceleration and $M_{i-1_{\epsilon M_{i-1}R_i}}$ is the linear acceleration, $M_{i-1_{\underline{\cdot}\,M_{i-1}R_i}}$ is the real part of the relative angular accelera tion $M_{i-1_{\underline{v}\,M_{i-1}R_i}}$ which is dependent on the generalised joint states $q_i, \dot{q}_i t$. $M_{i-1_{\epsilon}}$ is the real part of the relative linear accelera $^{r_{M_{i-1}R_i}}$ which is dependent on the generalised joint states $q_i, \dot{q}_i t$.

The advantage of using relative kinematics is that the equations of motions are dependent on a smaller set of generalised coordinates. For open kinematic chains, the number of generalised coordinates equates to the number of degrees of freedom in the system. Throughout, X is positive towards the front of the vehicle facing the direction of travel, Y is positive from the right to the left side of the vehicle and Z is positive up.

Motion performance

The acceleration data within the model can be taken at any point on any moving body or indeed a virtual centre. Examples within this paper are taken at the relevant seat rail attachment to the vehicle structure. The accelerations recorded are processed with weighted functions to ISO2631 W_f (ISO2631-1, 1997), for X, Y and Z directions, as shown in Figure 10.

The motion data illustrated are combined in equation (10) to from the numerator of the sickness equation (equation (12))

$$A_c = \sqrt{(X_{W_f} SX)^2 + (Y_{W_f} SY)^2 + (Z_{W_f} SZ)^2} \quad (10)$$

where A_c is root sum of square for the weighted acceleration to ISO2631 and W_f and SX, SY and SZ are scale factors used to expose contributions during target setting (default = 1.0).

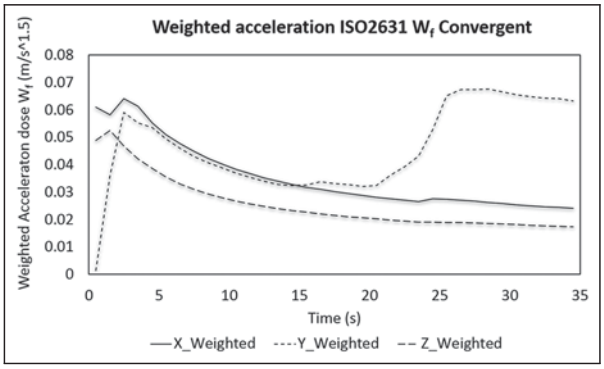

Figure 10. Modelled motion data, ISO2631 W_f weighting.

The convergent plotted output is more useful than the single value used in the literature when a sequence of vehicle manoeuvres is considered. Features in the weighted acceleration can be individually investigated and optimised to lower motion sickening motion. It is clear in the example shown above that there is an increase in the Y direction weighted acceleration following a manoeuvre in the time domain at 25 s. Having the ability to align discrete cause and effect is invaluable during the general tuning process of vehicles.

Task sequence

The task within the model follows a sequence of looking forward, reading, looking around and outside of the cabin, and then returning to a looking forward with gaze down. The reading part and looking around the cabin are achieved by eye motions and contraction of digital muscles in the neck to provide rotation and tilt of the head, as shown in Figure 11 (bottom). In addition to the neck motion, the head is also rotated at the skull to cervical C1 connection; this function is illustrated in Figure 11 (right).

The eyes are engineered to track a small ball within the cabin that initially scans a page of a tablet or book reading line by line. The target position relative to the head position is illustrated in Figure 11 (left). The ball in time travels outside of the vehicle in virtual space to entice the eyes to track and follow. The ball then returns to the forward position for the last segment and thus returns the head orientation and eyes back to the start point by relaxing the force in the neck controlling open loop forces.

This pragmatic modelling approach to head and eye movement can be extended to target-specific locations within the vehicle to evaluate the differences between information devices and obscuration from peripheral vehicle structure, for example. When all the motions are assembled, snapshots are illustrated, as shown in Table 2.

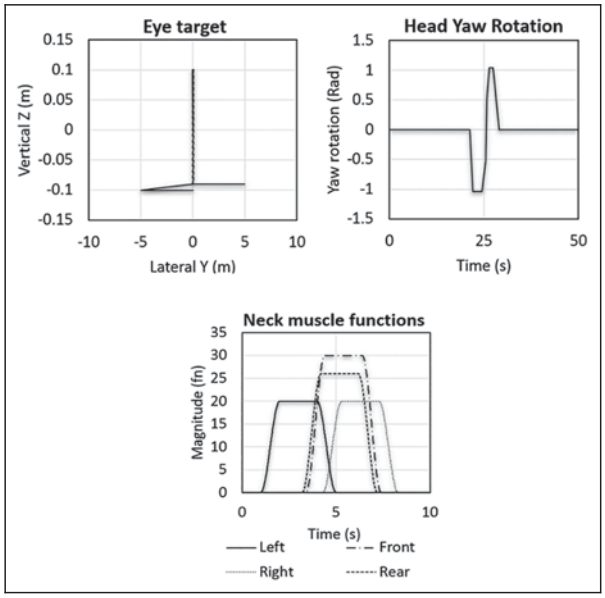

Figure 11. (Left) Eye target position, (middle) head rotation and (right) neck muscle functions.

Table 2. Modelled task timing.

Forward + tilt up	Reading	Right	Left	Forward + tilt down
0–10 s	10–20 s	20–25 s	25–30 s	30–35 s

Visual performance

The visual performance of the design is captured with virtual cameras tracking the digital occupant's eye view. The image is rendered into a video 1920 3 1080 pixels at 30 fps. It is widely reported in the literature that a view of the horizon is beneficial for motion sickness and general quantity of outward vision.[19] Within the digital environment, there is a wall 10 m high with a 2 km diameter with the origin at the start of the test track. This is coloured red. Any obscuring elements in the design of the vehicle, large seats, headrests and small windows will influence the amount of the red wall visible in the final rendered video output. The rendered videos of the sequence are then processed using a unique algorithm within MATLAB®.

The algorithm takes each frame from the video and calculates the percentage of each frame that contains red (horizon), green (vehicle structures), grey (road surface) and blue (sky) pixels. The algorithm output percentages of each visual component against the time base into an ASCII file for further processing.

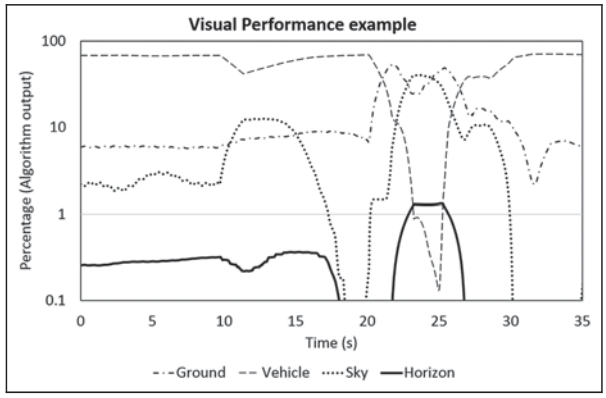

Figure 12. Measured output from the eye camera for ground, vehicle, sky and horizon.

It should also be noted that the results of this type of analysis are closely coupled to the virtual camera settings within the model. Lens parameters that control the field of view and focal lengths are influential in creating the geometry used for the visual processing. Both were kept constant within this research and may yield different results if replicated in another geometric rendering package. The key parameter in the package used is the 'lens angle'.[34] This was kept constant at 43° throughout.

An example output from the video processing is illustrated in Figure 12. Inspection of the reading section shows the degradation in horizon channel and also the head tilt . 27 s. The section looking around and out of the window 22–25 s indicates a clear improvement in the visible horizon. The looking down element of this sequence reduces the horizon to zero leaving a high percentage of vehicle obscuration and only some ground visible to the occupant.

The above data (Figure 12) can then be weighted to provide a summed quantitative value for the visual aspect of the digital drive. An initial estimation of the weightings was developed using a simple goal seek to minimise error for both looking up and looking down modalities from a physical trial n = 94. Normalising subjective sickness scores coupled with measured motion levels, there is a significant difference between looking up and down modalities highlighted by a t-test ($t = 26.6$, $p < 0.05$, Mean = 32.0, SD = 6.29, Mean = 48.6, SD = 16.2) for looking up and down, respectively. Using the images taken for looking up and looking down, as shown in Figure 13, the weightings were optimised until there was good agreement between the predicted and measured difference in sickness for both looking up and down conditions for the data illustrated in Figure 14.

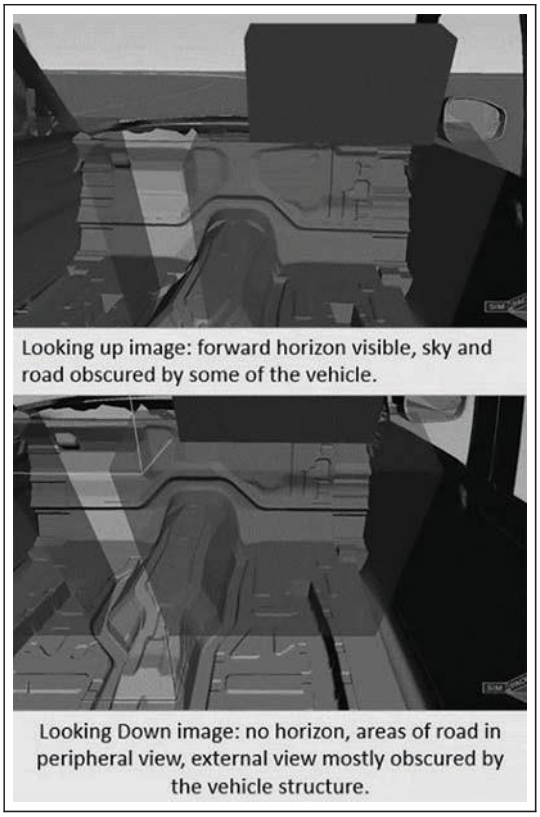

Figure 13. Looking up and down images used to optimise the weightings: (top) looking up and (bottom) looking down.

(Note that the weightings will change if the virtual lens angle is adjusted. Virtual lens angle is maintained throughout at 43° within this study). The resulting optimised weighting is shown in Table 3.

The logic for the above weightings is as follows. The literature has shown that the horizon is an important element and should dominate any antidote.[35,36] The horizon, therefore, has a larger weighting reflecting the published importance and the relatively small number of pixels that describe the horizon. The method only generates a small horizon signal, the 10 m tall red wall is around a kilometre away from the vehicle, and therefore, only a relatively small amount of the screen can be recorded as the horizon. The sky view is uncontrollable within a physical experiment. Clouds can be different for each participant in any outdoor trial where distant clouds move slowly relative to the vehicle but offer a contrasting object for orientation of pitch roll and yaw. This fact could be a significant source of experimental noise between participants. As such, a weighting factor of 2 is used in the model. The ground view will be closer to the vehicle, and although positive in that it is a view outside, there is the possibility that strobing, forced rapid eye tracking could lead to a level of visually induced motion sickness (VIMS), an initial proposal of 1 is used here.[37] The level of obscuration by the vehicle is negative with an initial weighting of 1 (minus). Future studies will inevitably allow further optimization of the weightings. It is suggested that the anticipation of the future path of the vehicle is important for the levels of motion sickness observed.[38] To facilitate this, a simple function that uses the yaw angle of the head and of the vehicle determines if the occupant could view the preview marker at 40 m ahead of the vehicle which is also limited by the vehicle structure. A 40 m preview distance provides stable yaw gain for normal speeds and road geometry.[39] An example of the anticipatory function for forward and rearward seating orientation including an obstacle is illustrated in Figure 15. Within this present study, the anticipatory function An(t) only applies to the horizon function. The forward horizon graded by the anticipation func- tion replicates where a trained driver observes the apex for vehicle control.[40]

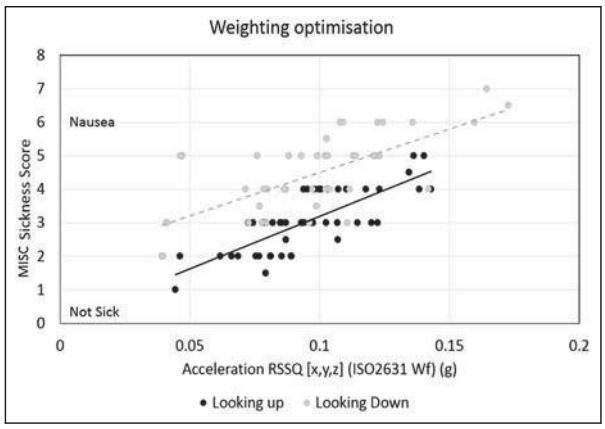

Figure 14. Sickness data used to optimise the vision weightings in predevelopment: 0 = no sickness, 10 = emesis (MISC).

The visual attributes are combined using the function $V_c(t)$ for t = (1, 2, ... T) is regarded as the weighted sum of observations in equation (11)

$$V_c(t) = (s(t) \cdot s_w + \tfrac{1}{2}(h(t) \cdot h_w) \cdot An(t) \cdot An_w + gr(t) \cdot gr_w - o(t) \cdot o_w) \quad (11)$$

where S(t) is sky percentage (%) as a function of time, s_w is sky scene component weighting (Table 3), h(t) is horizon percentage (%) as a function of time, h_w is horizon scene component weighting (Table 3), gr(t) is ground percentage (%) as a function of time, gr_w is ground scene component weighting (Table 3), o(t) is obscuration percentage (%), o_w is obscuration weighting (Table 3), An(t) is anticipatory function, An_w is weighting and $\sum_{t=i} S(t) + h(t) + o(t) = 100\%$.

Sickness processing

A unique algorithm is proposed to take the results from the vision and motion data and combine it into a time sequence. The resulting output is a time-based accumulation of motion dose A_c (numerator) adjusted by the level of external vision quality V_c (denominator) VA_c (equation (12)). If there is sickening motion and there

Table 3. Initial weightings developed from predevelopment experiments.

Scene component	Ground (gr_w)	Obscuration (vehicle) (O_w)	Sky (s_s)	Horizon (h_w)
Weighting	1	1	2	10

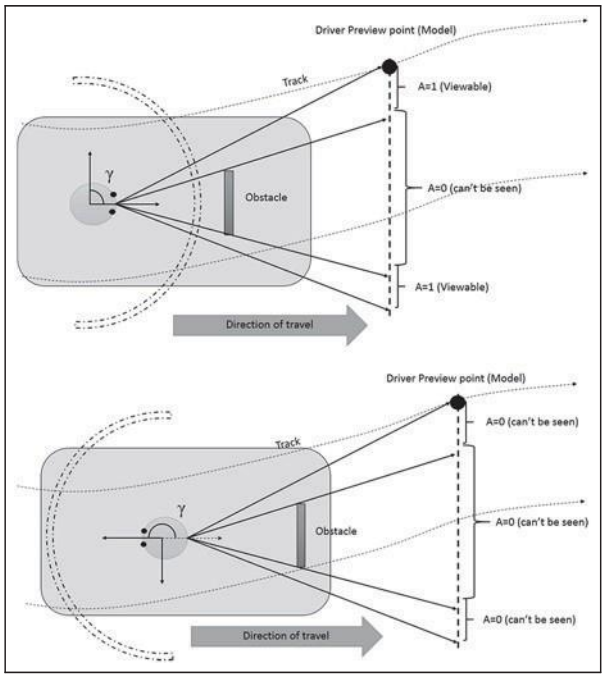

Figure 15. Anticipatory function: (top) facing forwards and (bottom) facing rearwards.
If the driver preview marker is not viewable from a combination of head rotation (g) and field of view, then A = 0; if the driver preview marker is visible, then A = 1. Dot–dash denotes the field of view for each seat position.

is no external view, sickness is generated. If there is motion and enough external view determined by V_c, then motion sickness levels VA_c will be reduced

$$VA_c(t) = \frac{\left(\frac{XYZ_{W_f}}{S(XYZ)}\right) \cdot V_c}{V_c \cdot V_s + V_g} \delta t \qquad (12)$$

where XYZ_{W_f} is from ISO2631 (14), S(XYZ) is scale factor (default = 1.0), V_c is visual signal (equation (11)) and V_g is visual geometry offset (100.0), used to ensure that all values are positive for conditions when the external view is completely obscured by the vehicle interior. Complete obscuration would lead to a value of 2100. V_s is visual scale factor (1.0), used to modify the balance of vision to motion for target setting and influence.

There is an inevitable interaction where the visual performance is influenced by the head motion which is in turn a result of the vehicle motion. The results currently reflect a passive occupant in the vehicle, where in some cases the occupants could brace and counteract

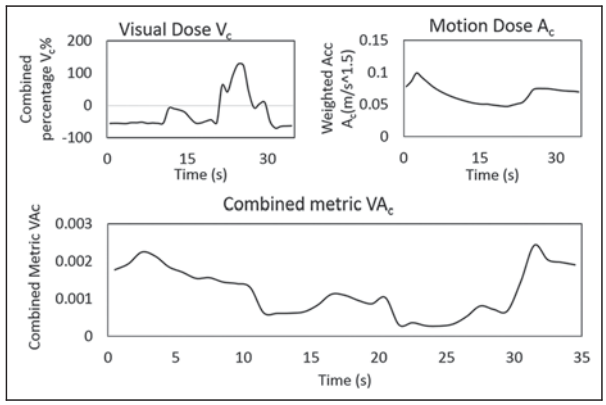

Figure 16. (Top left) Example of vision, (top right) motion and (bottom) the combined sequence for motion sickness.

the head motion in response to the vehicle motion, this is not considered here.

Amalgamating the data for visual performance and the weighted acceleration in a single time-based metric for motion sickness is presented in Figure 16 (bottom).

Benchmarking of five vehicles for motion sickness performance has shown that lower and negative values of VA_c indicate better motion sickness performance. A survey consisting of over 500,000 miles of real-world sickness data was used to grade the motion sickness performance using the MISC scores for general social and domestic pleasure driving.[10] The subjective MISC scores are compared to the modelled equivalent and illustrated in Figure 17.

Analysis of variance (ANOVA) indicates a significant relationship between the subjective sickness scores recorded and the modelled equivalent ($F = 57.8$, $r^2_{adjusted} = 0$:93, $p < 0.001$, Mean = 0.19, SD = 0.05, Mean = 0.005, SD = 0.193) for subject and modelled results.

Thresholds will need to be developed following further research leading to workable targets for specific acceptance against the cost of mitigation. Meaning, premium vehicles could afford more mitigation and therefore be acceptable with higher levels of VA_c from base vehicle performance. The resulting combined sequence can then be accumulated over time to predict motion sickness damage over time equivalent to MISC scores for a subjective experiment (equation (13)). Further filtering could be added at this juncture to account for susceptibility (f(MSSQ)) if needed

$$MISC_{predicted} = \sum_{n=0}^{T} VA_c(n)(n+1) \cdot f(MSSQ) \qquad (13)$$

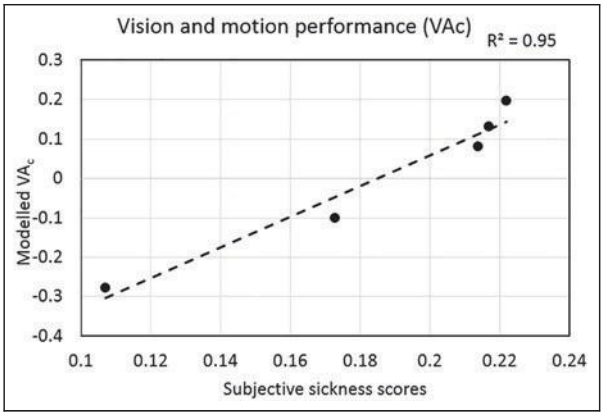

Figure 17. VA_c performance of five different vehicles (saloons and luxury 4 3 4) compared to subjective sickness performance for the same set of vehicles.

where VA_c is sampled in every $t = 2$ s.

Within this method, the calibration between subjective and objective data sets is adjusted within the weightings of the visual components for 2 s intervals during the summation of the MISC scores. $MISC_{predicted}$ scores are presented for the two case stud- ies in the results section. As previously stated, the weightings derived for this present study were gener- ated within predevelopment using goal seeking to reduce comparative error between the subjective data and model data.

Results

Results for three case studies are presented; first, a study to demonstrate and verify that the model is capa- ble for predicting sickness scores at numerous head positions within the cabin. Second, validation of the model using a seating orientation study is presented to demonstrate the importance of the future path of the vehicle.[41] Third, validation of the model to an independent study investigating display height and motion sickness that is useful for non-driving-related tasks (NDRTs) in future AVs.[17]

Case study A: sickness performance within a vehicle

Using the model described in this present study, the sickness levels at numerous positions within a conventional vehicle cabin were evaluated. The levels of predicted sickness at each position are illustrated in Figure 18. The relative size of the spheres indicates the level of sickness at each position due to a combination of motion, vision and task (Table 2).

Consequently, there is a significant difference between the predicted sickness for front and rear scores (MISC) ($T = 29.64$, $p < 0.001$, $Mean = 0.53$, $SD = 0.03$, $Mean = 0.95$, $SD = 0.16$) for averaged front and rear seating positions, respectively, as shown in Figure 19. This is congruent with findings in real-world studies in passenger vehicles[21] where it is known that the rear of vehicle generates more sickness incidence due to reduced external vision.

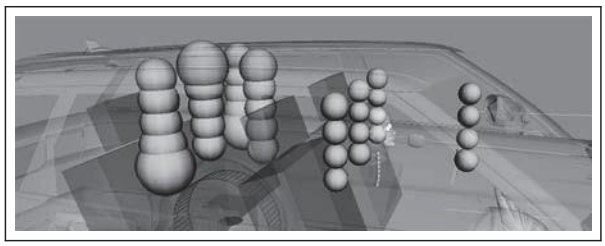

Figure 18. Predicted sickness at locations within a vehicle cabin, relative magnitude is indicated by the size of the spheres.

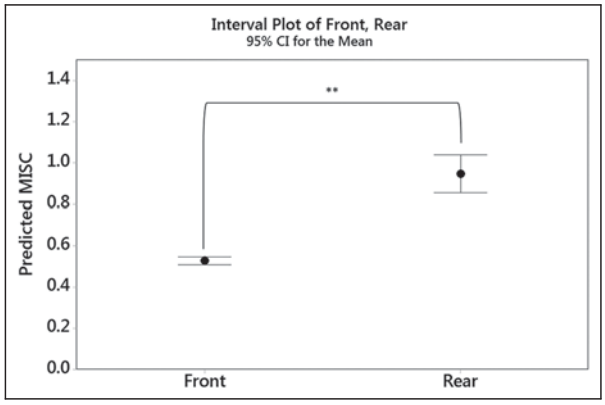

Figure 19. Comparisons of the means for predicted sickness (MISC) for front and rear positions.

Case study B: seating orientation

Introduction. In a recent study, motion sickness was evaluated with respect to seating orientation using an autonomous vehicle concept in an urban environment.[18] The environment and vehicle are replicated in this study and compared to the results of the real experiment.

Method. A detailed model was created of the vehicle within a MBS software package. The model replicated the physical vehicle for seating positions and obscuration of the exterior view. Dynamic performance of the model was matched to the measured vehicle response over the test surface. The driver model used a preview distance of 40 m for lateral track control using default driver model parameters, as shown in Figure 20 (top and bottom).

Weightings for the visual equations are listed in Table 3. A track was created within the model to replicate the geometry used in the physical experiment, as shown in Figure 21.

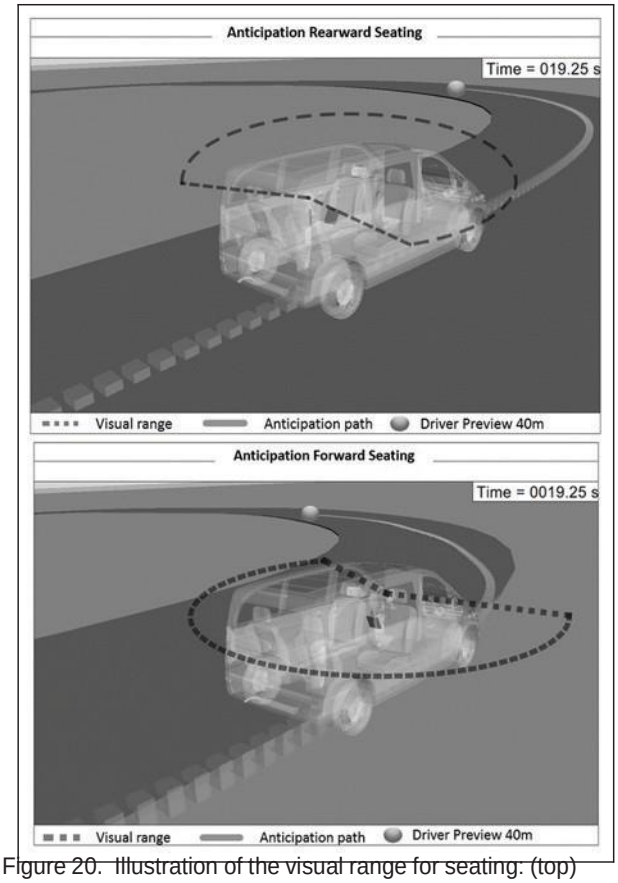

Figure 20. Illustration of the visual range for seating: (top) forwards (blue graphic) and (bottom) rearwards.

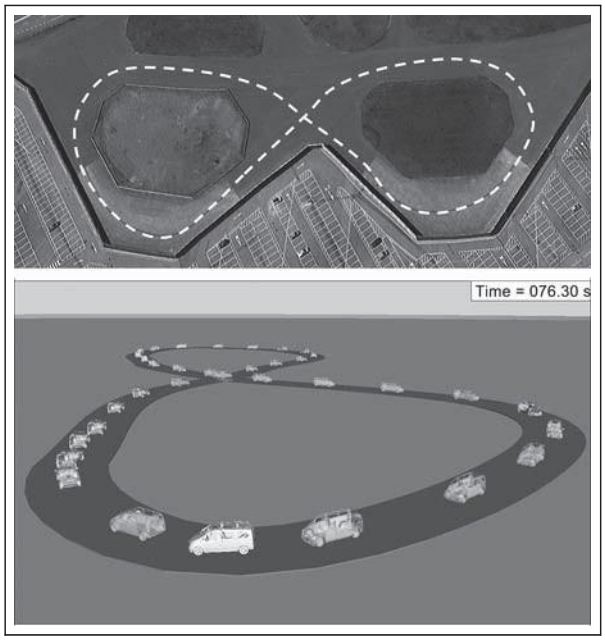

Figure 21. Track layout: (top) physical and (bottom) model.

Stimuli. The model was driven around with a target velocity of 25 km/h for 15 min. There were 10 repeats of the loop within that time. Braking and acceleration

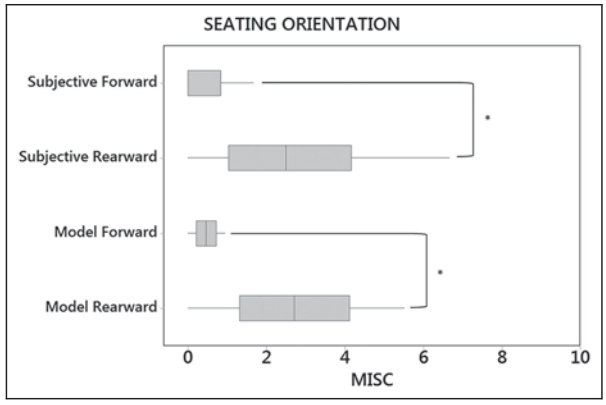

Figure 22. Model to subjective MISC scores for seating forwards and rearwards.

matched the physical test at the intersection of the loops.

Task (described in section 'Task sequence'). In this example, the standard reading task previously described in sec- tion 'Task sequence' was used for the first 50 s, fol- lowed by gaze forward or rearward for the remainder of the analysis. In the physical test, occupants were free to conduct a meeting with some limited gaze down activities.

Results. A comparison was made between the accelerations taken from the study as to those developed by the model for the urban section. There were no significant differences found between the measured and predicted accelerations using a t-test ($T = 21.02$, $p = 0.31$, $T = 0.37$, $p = 0.7$) for longitudinal and lateral directions (Mean = 0.0, SD = 0.119, Mean = 0.0, SD = 0.071), for the model and measured longitudinal motion (Mean = 0.0, SD = 0.125, Mean = 0.0, SD = 0.183) and for the model and measured lateral motion, respectively. The track is flat and smooth and as such did not generate any notable vertical accelerations when weighted for motion sickness frequencies, (Mean = 0.0, SD = 0.0, Mean = 0.0, SD = 0.06) for vertical motion from the model and physical measurements, respectively, when normalised for gravity. Processing and comparing the data for predicted sickness using equations (10)–(12) to subjective scores from the physical test, the resulting sickness scores are illustrated in Figure 22.

There was a significant difference recorded by both the model and subjective data between forward and rearward orientations, as shown in Table 4.

Without the anticipatory function, sitting rearwards is slightly improved over the forward view because of the improved exterior view without the driver privacy screen, as shown in Figure 23 and Table 5.

Discussion. With this example, it is shown that there is agreement between the model and the subjective study for seating orientation for recorded levels of sickness.

Table 4. Model to subjective MISC scores for seating forwards and rearwards t-test results.

M (model) S (subjective)	M(F) M(R)	S(F) S(R)	M(R) S(R)	M(F) S(F)	M(R) S(F)	M(F) S(R)
t p	–30.03 0.0	–4.71 0.0	–0.5 0.62	0.1 0.923	–8.91 **< 0.0**	–5.7 **< 0.0**
R (rearward) F (forward)	S(F)	S(R)	M(F)	M(R)		
Mean SD	0.49 0.83	2.53 1.78	0.46 0.27	2.72 1.61		

MISC: MIsery Sickness sCale; SD: standard deviation.
p < 0.05; values in bold signifies the smallest value of p.

Table 5. Modelled MISC with and without anticipatory function, t-test results.

t-test	Forward to rearward	Forward to rearward (no anticipatory cue)	Forward to rearward (no anticipatory cue)
t p	30.03 **< 0.0**	19.01 **< 0.0**	33.88 **< 0.0**
	Forward	Rearward with anticipation function	Rearward without anticipation function
Mean SD	0.46 0.27	2.72 1.61	0.20 0.12

MISC: MIsery Sickness sCale; SD: standard deviation.
p < 0.05; values in bold signifies the smallest value of p.

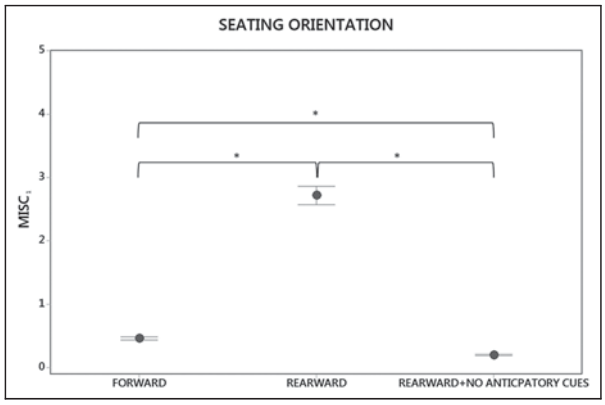

Figure 23. Predicted sickness with and without anticipatory function.

The anticipatory function is key to reconciling seating orientation. If the results are processed without the anticipatory function, the rearward results are no different to the forward results in this present study, noting the model has enough resolution to determine the differences between front and rearward exterior views from the occupant seating positions using the same inputs.

The model can determine vision attributes independently to vehicle motion and vice versa with clinical precision that are repeatable and free from experimental error. The weightings were developed to match 65th percentile susceptibility using MSSQ Short.[42] Further developments will be aimed at refining normalised weightings and applying a global susceptibility parameter for gender, age and ethnicity.

Case study C: display height

Introduction. A detailed and appropriate study has been published that investigates the height of displays with respect to the MISC scores for a slalom test.[17]

Method. Using the method described in the original paper, this model will be used to replicate the physical experiment. The vehicle used in the original study is a VW Passat; the model uses a Jaguar XE vehicle for comparison. Both have similar overall dimensions; however, there will be obvious visual differences. In addition, there is little detail for the circular path and speed for the vehicle at the ends of the slalom test. There will be a significant contributor to MISC if the speed is high and radius of turn is small, as shown in Figure 24 (bottom). Two conditions are considered, a high screen and low screen viewed for 900 s when driven at the prescribed speeds by the original study (25 km/h).

Within this study, independent recorded real-world MISC scores were used to further refine the vision weightings, as shown in Table 6.

The adjustments to the visual weightings were minor and not significant ($t = 0.48$, $p > 0.05$). Future adjustments will be made to the weightings as more data for other MISC-based experiments become available.

Results. The predicted output from this model when replicating the known conditions of the Kuiper et al.[17] study is illustrated in Figure 25.

Completing a t-test between the model and Kuiper's subjective data shows strong agreement for both relative and absolute levels, as shown in Figure 26 and Table 7. The subjective MISC scores between the model and the physical experiment indicate a significance difference between high and low display heights.

Table 6. Visual weightings, originally developed from other studies, including optimised weightings for this study.

	Ground (S_{VG})	Vehicle (S_{VV})	Horizon (S_{VH})	Sky (S_{VS})
Original	1	1	10	2
Optimised	1	0.9	10	1.5

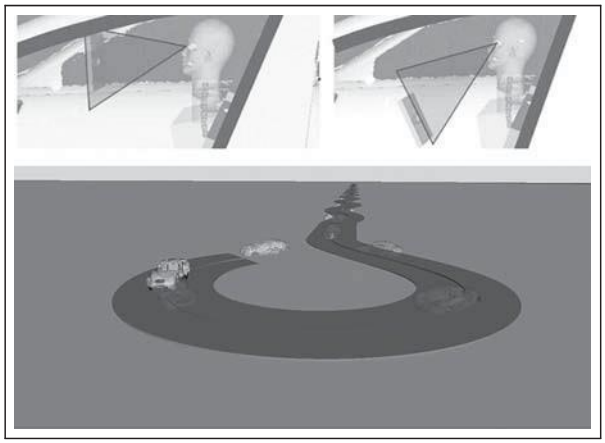

Figure 24. Model images: (top) participant task and (bottom) road geometry.

Discussion. Validation of the method to an independent study has been shown in this present case study. There is a strong agreement between the predicted MISC scores from model to the MISC scores recorded by Kuiper et al. Better definition of the motion at the ends of the slalom would be an advantage in reproducing the original study. Nonetheless, the model provides absolute and relative differences between the two dis- play heights indicative of the physical study.

The vision weightings for the model were optimised, although not essential, the modified weightings presented in this case study represent both n = 94 from the original predevelopment with the addition of n = 15 from this test. Future refinements using other published studies will further enhance the accuracy of the model for the general population.

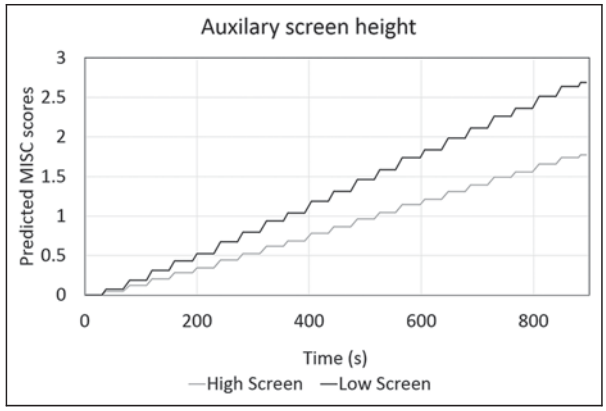

Figure 25. Predicted sickness scores for the two considered screen heights (high and low).

Table 7. t-test between this model and Kuiper's results, H (high), L (low), K (Kuiper), M (model).

	Within methods		Between methods			
	H(K) L(K)	H(M) L(M)	H(M) H(K)	L(M) L(K)	L(K) H(M)	H(K) L(M)
t	2.44	–8.89	0.7	0.86	3.24	–2.39
p	**\ 0.015**	**\ 0.0**	0.495	0.4	**\ 0.001**	**\ 0.017**

p \ 0.05; values in bold signifies the smallest value of p.

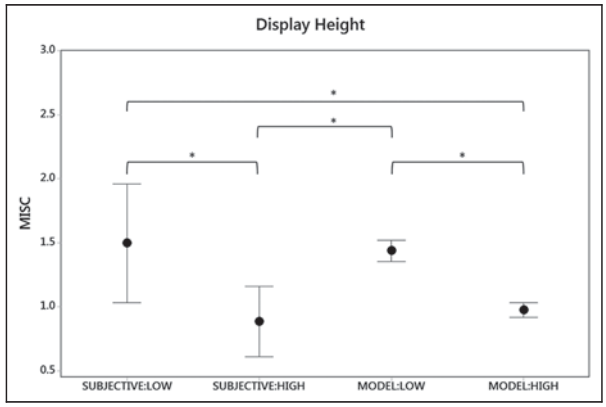

Figure 26. Agreement between this study and Kuiper's results (subjective = Kuiper study).

Discussion

The results from case study A are congruent with real-world subjective evaluations by Griffin[20] where it was shown that improved forward vision from front seating positions provide a marked improvement in sickness reported. Additional validation has been provided with two additional studies B and C. In both, the model can predict both absolute and relative sickness levels for two proven factors that lead to increased motion sickness incidence.

Flexural modes of the vehicle structure and large mass systems are not influential in motion sickness dynamics. Wheel and power-unit modes are typically 10–15 Hz. The vertical response of normal passenger vehicles are typically of the order of around 1–1.5 Hz,[43] an order of magnitude above motion sickness sensitivity. It is, however, essential to provide an accurate representation of any driver controls for steering, braking and acceleration. Changes to direction or speed by the driver introduce state changes that inevitably result in ultra-low frequency motion that are known to cause motion sickness. Vehicle control has been proven to be influential to motion sickness levels.[21] Accurate and representative vehicle 3D geometry is needed to disrupt

the external view and limit the antidote of earth fixed reference.

ISO2631 W_f filtering is used for fore-aft, longitudinal and vertical directions. Revisions are necessary to the published standards similar to those proposed[15] or similar. A simple Tschebyshev band pass filter has provided good correlation to objective and subjective measures in another study.[44] The model is independent of the motion weighting functions and any can be applied during the post-processing stages. There is current research taking place (2019) to establish a unified set of weightings for motion sickness within passenger vehicles.

The vision weightings can be adjusted to reflect the susceptibility of the target sample. The weightings used in this study reflect 65th percentiles MSSQ Short.[42] The adjustments made between case studies A, B and C albeit small may reflect the susceptibility differences between the participants within the Kuiper et al.[17] study to those participants from predevelopment studies in development of the weightings used in case studies A and B.

The sickness scores generated within this model will, if the motion is not counteracted sufficiently by the vision, continue to rise beyond conventional MISC scoring. Practically within research, participants terminate tests at values around 6. Occupants although rare terminate at emesis with a MISC score of 10. The benefit of the model in its current form is that vehicle design and motion control attributes can be evaluated in advance of prototype vehicles for motion sickness. Either by looking at absolute levels of sickness for a specific route and task but also the length of time taken to develop nausea (MISC = 6). If vehicles are improved, the time to nausea can be extended leading to a greater chance of habituation and/or simply more time completing NDRT's adding inherent value to that journey pre-nausea.

Within this model, the task and environment are completely flexible and can be matched to any physical test. One clear advantage of a 'virtual' model for motion sickness is that the results are not susceptible to human variability, vehicle and environment noise that lead to experimental error. All physical test methods used within this research meet measurement systems analysis (MSA) standards. Both vision and motion benchmarking techniques are below 5% variation for reliability and repeatability.[45]

In addition, the model can also be used to evaluate route choice for onboard navigation options to not only offer the most efficient for energy and time but also comfort and wellbeing depending on the selected intended tasks. For example, if occupants select office-based tasks, routes can be chosen to limit the build of motion sickness and routes that impose less lateral motion and therefore increase task performance.

Interestingly, in other studies using the model, battery electric vehicles (BEVs) are shown to be less provocative in the longitudinal direction under acceleration. BEVs have no discernible gear shuffle compared to both manual and automatic internal combustion engines (ICE). However, BEV regenerative braking can cause provocative levels of deceleration that lead to motion sickness. Care will be needed to balance energy recovery versus comfort/wellbeing requirements, particularly, for the initial exposure of full BEV and AVs to the general population. It may be useful, for example, to gradually introduce regenerative braking over several minutes until passengers are accus- tomed to the increased braking sensations. Adaptation is a proven method for motion sickness mitigation.[22]

The model will be further developed to include a suite of NDRTs to validate a range of multi-tasking scenarios within future AVs using a design of experiments (DOE) approach. Computation of anticipatory cues and augmented reality of the future path will be included to ensure that future vehicle designs maximise the view and uptake of motion sickness antidotes while occupants multitask in any seating position.

This paper describes a novel method for establishing motion sickness potential for vehicle design, motion control and occupant tasks eliminating the need for prototype vehicles.

Conclusion

The novel model demonstrated here can determine significant differences in vehicle design for motion sickness for display heights and seating orientation. In addition, the model can significantly rank the sickness performance of five vehicles using more than 0.5M miles of real-world driving.

Reproducibility

As stated previously, the weightings used for vision are optimised to a study for looking up and down modalities with a mean susceptibility of 65th percentile.[41] Comparisons to other studies with different susceptibility, the weightings shared here may not be appropriate. In addition, the vision outputs specific to the software's interpretation of the 3D virtual environment and may generate differing results if rendered in other software.

Declaration of conflicting interests

The author(s) declared no potential conflicts of interest with respect to the research, authorship, and/or publication of this article.

Ethical approval

Ethics for predevelopment and supplementary data used within this research are covered by Coventry University code of ethics P65727, P65717, P76439 and P76213.

Funding

The author(s) disclosed receipt of the following financial support for the research, authorship, and/or publication of this article: This work was supported by Jaguar Landrover forming part of a full time PhD in Autonomous vehicle motion sickness at Coventry University, United Kingdom.

ORCID iD

Spencer Salter https://orcid.org/0000-0001-6379- 6753

References

1. St-Louis E, Manaugh K, Van Lierop D, et al. The happy commuter: a comparison of commuter satisfaction across modes. Transport Res F-Traf 2014; 26: 160–170.
2. MacKenzie D, Wadud Z and Leiby P. A first order estimate of energy impacts of automated vehicles in the United States. In: Proceedings of the transportation research board annual meeting, Washington, DC, 12–16 January 2014.
3. Griffin MJ and Hayward RA. Effects of horizontal whole-body vibration on reading. Appl Ergon 1994; 25: 165–169.
4. Mansfield N, Arora Y and Rimell A. Computer use on moving trains: which pointing device? Contemp Ergon 2007; 2007: 255–260.
5. Narayanamoorthy R and Huzur Saran V. Error analysis of task performance with laptop in vibration environment. Comput Human Behav 2011; 27: 2263–2270.
6. Sundströ m J and Khan S. Influence of stationary lateral vibrations on train passengers' difficulty to read and write. Appl Ergon 2008; 39: 710–718.
7. Diels C and Bos JE. Self-driving carsickness. Appl Ergon 2016; 53: 374–382.
8. Reason JT and Brand JJ. Motion sickness. Oxford: Academic Press, 1975.
9. Dobie TG. Motion sickness: a motion adaptation syndrome. Cham: Springer, 2019, p.302.
10. Keshavarz B and Hecht H. Validating an efficient method to quantify motion sickness. Hum Factors 2011; 53: 415–426.
11. Bos JE, Mackinnon SN and Patterson A. Motion sickness symptoms in a ship motion simulator: effects of inside, outside, and no view. Aviat Space Environ Med 2005; 76: 1111–1118.
12. Bullinger HJ, Warschat J and Fischer D. Rapid product development: an overview. Comput Ind 2000; 42: 99–108.
13. BS 6841. Guide to Measurement and evaluation of human exposure to whole-body mechanical vibration and repeated shock. London: British Standards Institution, 1987.
14. ISO 2631-1: mechanical vibration and shock: evaluation of human exposure to whole-body vibration, 1997, https://www.saiglobal.com/PDFTemp/Previews/OSH/ISO/ISO_12345_05-01/T007612E.PDF
15. Donohew B and Griffin MJ. Motion sickness: effect of the frequency of lateral oscillation. Aviat Space Environ Med 2004; 75: 649–656.
16. Turner M and Griffin MJ. Motion sickness in public road transport: passenger behavior and susceptibility. Ergonomics 1999; 42: 444–461.
17. Kuiper OX, Bos JE and Diels C. Looking forward: in-vehicle auxiliary display positioning affects carsickness. Appl Ergon 2018; 68: 169–175.
18. Salter S, Diels C, Herriotts P, et al. Motion sickness in automated vehicles with forward and rearward facing seating orientations. Appl Ergon 2019; 78: 54–61.
19. Diels C. Will autonomous vehicles make us sick? In: Sharples S and Shorrock S (eds) Contemporary ergonomics and human factors. Boca Raton, FL: CRC Press, 2014, pp.301–307.
20. Griffin MJ and Newman MM. Visual field effects on motion sickness in cars. Aviat Sp Environ Med 2004; 75: 739–748.
21. Turner M and Griffin MJ. Motion sickness in public road transport: the effect of driver, route and vehicle. Ergonomics 1999; 42: 1646–1664.
22. McCauley ME, Royal JW, Wylie CD, et al. Motion sickness incidence: exploratory studies of habituation, pitch and roll, and the refinement of a mathematical model, 1976, https://trid.trb.org/view/399367
23. De Graaf B, Bles W and Bos JE. Roll motion stimuli: sensory conflict, perceptual weighting and motion sickness. Brain Res Bull 1998; 47: 489–495.
24. Bles W, Bos JE, De Graaf B, et al. Motion sickness: only one provocative conflict? Brain Res Bull 1998; 47: 481–487.
25. Wada T, Fujisawa S and Doi S. Analysis of driver's head tilt using a mathematical model of motion sickness. Int J Ind Ergon 2018; 63: 89–97.
26. Dorsch V. Simulation of vehicle dynamics control by active steering systems. In: Proceedings of the SIMPACK user meeting, 2014, http://www.simpack.com/fileadmin/simpack/doc/usermeeting14/Day_2_Room-1/10_UM14_Ostfalia_Dorsch_Sim-Vehicle-Dyn-Control-Active-Steering-Sys.pdf
27. Rulka W and Eichberger A. SIMPACK an analysis and design tool for mechanical systems. Veh Syst Dyn 1993; 22: 122–126.
28. Salter SL. The use of SIMPACK on the all new Jaguar XK. SIMPACK News, February 2006, https://www.3ds.com/fileadmin/EVENTS/SIMULIA-Simpack/archiv-MBS-before2016/2006-MBS-SN-JLR-Salter.pdf
29. Salter SL. Uses of SIMPACK on the all new Land Rover discovery. In: Proceedings of the SIMPACK user meeting, 2004. Dassault Systemes Simulia Corporation, https://www.3ds.com/fileadmin/EVENTS/SIMULIA-Simpack/archiv-MBS-before2016/2004-SUM-JLR-Slater.pdf
30. Seherr-Thoss H-C, Schmelz F and Aucktor E. Universal joints and driveshafts: analysis, design, applications. New York: Springer Science & Business Media, 2006.
31. Manning WJ and Crolla DA. A review of yaw rate and sideslip controllers for passenger vehicles. T I Meas Control 2007; 2: 117–135.
32. Harty D. The myth of accuracy. J Eng Integr Soc 2001; 9: 22–28.
33. Murray RM, Li Z and Sastry SS. A mathematical introduction to robotic manipulation (Vol. 29). Boca Raton, FL: CRC Press, 1994, p.480.
34. Dassault. SIMPACK 9.1 user guide, 9.10.2. Dassault Systemes Simulia Corporation, 2016, http://www.simpack.com/
35. Rolnick A and Bles W. Performance and well-being under tilting conditions: the effects of visual reference and artificial horizon. Aviat Sp Environ Med 1989; 60: 779–785.

36. Tal D, Gonen A, Wiener G, et al. Artificial horizon effects on motion sickness and performance. Otol Neurotol 2012; 33: 878–885.
37. Frank LH, Casali JG and Wierwille WW. Effects of visual display and motion system delays on operator performance and uneasiness in a driving simulator. Hum Factors 1988; 30: 201–217.
38. Feenstra PJ, Bos JE and Van Gent RNHW. A visual display enhancing comfort by counteracting airsickness. Displays 2011; 32: 194–200.
39. Sharp RS. Driver steering control and a new perspective on car handling qualities. Proc IMechE Part C: J Mechanical Engineering Science 2005; 219: 1041–1051.
40. Land MF and Tatler BW. Steering with the head: the visual strategy of a racing driver. Curr Biol 2001; 11: 1215–1220.
41. Salter S, Diels C, Herriotts P, et al. Motion sickness in automated vehicles with forward and rearward facing seating orientations. Appl Ergon 2019; 78: 54–61.
42. Golding JF. Predicting individual differences in motion sickness susceptibility by questionnaire. Pers Individ Dif 2006; 41: 237–248.
43. Sharp RS and Crolla DA. Road vehicle suspension system design: a review. Veh Syst Dyn 1987; 16: 167–192.
44. Salter S, Diels C, Thake D, et al. Motion sickness prediction device for automated vehicles. Int J Mech Produc Eng 2019; 7: 68–74.
45. Pyzdek T and Keller PA. The six sigma handbook (Vol. 4). New York: McGraw-Hill Education, 2014.